Energetic Particle dynamics induced by off-axis neutral beam injection on ASDEX Upgrade, JT-60SA and ITER

PH. LAUBER[1], V.-A. POPA[1], G. PAPP[1],T. HAYWARD-SCHNEIDER[1], G. MENG [1], Z. LU [1], EUROFUSION ENR NAT[2] AND MET[3] TEAMS,
B. GEIGER[4], L. GIL[5], G. D. CONWAY[1], M. MARASCHEK[1], AND THE ASDEX UPGRADE TEAM,
A. BIERWAGE[6], K. SHINOHARA[6,7], M.SCHNEIDER[8], S.D. PINCHES[8]

[1]MPI für Plasmaphysik, IPP, Germany
[2] see ENR NAT Team
[3] see ENR MET Team
[4] University of Wisconsin, Madison, USA
[5]Instituto de Plasmas e Fusao Nuclear, IST, Universidade de Lisboa, Lisboa, Portugal
[6] National Institutes for Quantum and Radiological Science and Technology, Naka Fusion Institute, Ibaraki311-0193, Japan
[7] The University of Tokyo, Kashiwa, Chiba 277-8561, Japan
[8] ITER Organization, Route de Vinon-sur-Verdon, CS90046, 13067 St Paul-lez-Durance, France

E-mail contact of the main author: philipp.lauber@ipp.mpg.de

1. ABSTRACT

In this paper we report on experimental and modeling results concerning the energetic particle (EP) dynamics in plasma scenarios with off-axis neutral beam (NB) injection at ASDEX Upgrade (AUG). Various hydrogen isotope mixes were chosen in order to enlarge the database for scaling studies, especially in the view of transitions between different EP transport regimes. The observed instabilities driven by spatial and phase-space gradients are identified and analysed applying a linear stability analysis. The tools developed and validated in this process are applied to selected scenarios on JT-60SA and ITER pre-fusion plasmas, focusing on first applications of a fully automated EP stability workflow.

2. INTRODUCTION

Off-axis NB injection is an important tool to control and optimise the current profile in both conventional and advanced tokamak scenarios. Via tailoring the safety factor profile, the positions of the rational surfaces can be controlled, the local magnetic shear can be changed or reversed shear regions can be established. Whereas in present devices the beam energies are typically 10-20 times larger than the plasma background temperature and the beam velocities are smaller than the Alfvén velocity ($v_{NB}/v_A \sim 0.3 - 0.4$), in future devices such as JT-60SA and ITER these ratios will go up to 100 for $E_{NB}/T_{thermal}$ and to $v_{NB}/v_A \gtrsim 1$. Thus, it is expected that the related EP-driven instabilities and the relaxation of the spatial EP pressure gradients will be different (e.g. mode number spectrum, non-linear saturation) than in present-day experiments. Off-axis drive introduces both a positive and a negative EP gradient region, causing instabilities that propagate in the electron diamagnetic direction (positive gradients) and ion diamagnetic direction (conventional negative EP gradient). The related EP transport is directed to deplete the gradients, i.e. inwards in the positive gradient region and outwards in the negative gradient region. Since the redistribution of the EP beam will affect the background plasma properties through various channels - e.g. the heating and current drive efficiency, in particular for the ramp-up and ramp-down phases - it can be tested if the stability predictions and the related EP transport calculations are able to catch the experimental signatures and thus can be used with confidence in future comprehensive scenario simulations.

3. ASDEX UPGRADE: ENERGETIC PARTICLE DYNAMICS IN DIFFERENT ISOTOPE PLASMAS

In 2017 a new scenario on ASDEX Upgrade has been established for the dedicated investigation of EP physics [1] that is optimised to maximise β_{EP}/β_{th} and the ratio $v_{NB}/v_{thermal}$. This scenario has been recently further developed into both an L-mode and an H-mode scenario with stable flat-top phases and with more complete diagnostic coverage. In addition to the standard deuterium (D) discharges, hydrogen (H) experiments and mixed D,H discharges were conducted, where D beams were injected into an H plasma, resulting in a 70:30 H:D ratio. As in the previous discharges, impurities (mainly tungsten) accumulate in the core since no central heating is supplied. Due to strong radiation losses the background temperatures and pressures of both ions and electrons stay low, despite $2.5 - 5$ MW NB heating. Under these conditions both ion and electron Landau damping are reduced, and strongly non-linear EP dynamics can be observed in most of the dedicated discharges. Adding stepwise core ECRH heating (not discussed here in detail) allows us to determine the thresholds for the existence conditions of the phenomena under investigation.

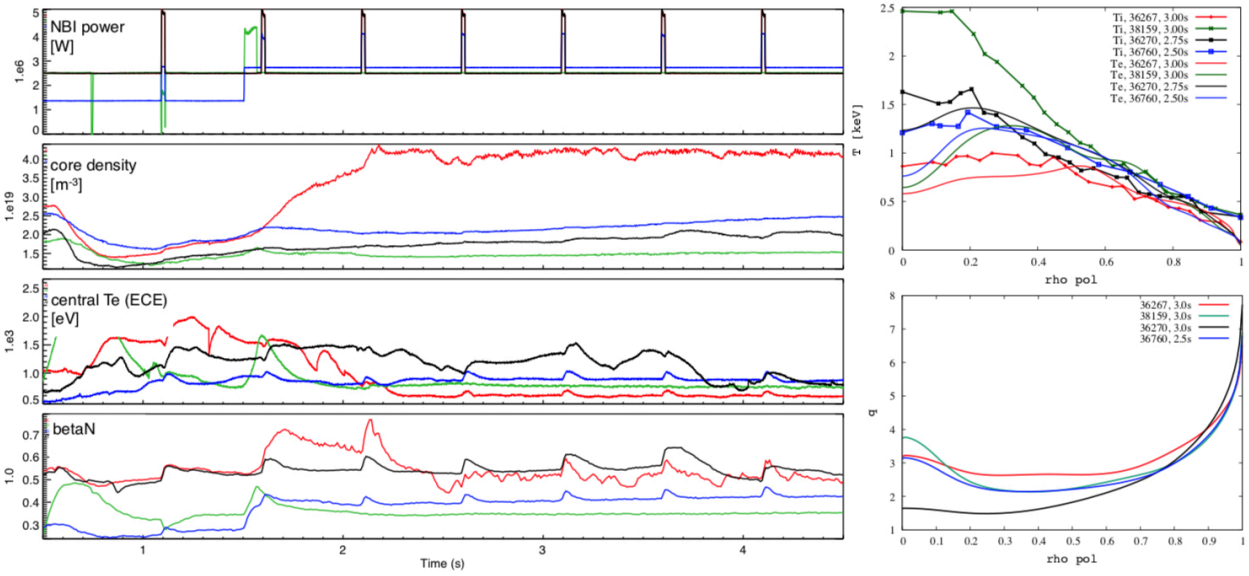

FIG. 1. Left: time traces of 3 L-mode and one H-mode discharges in different isotope mixes and heating powers. Red: #36267, D → D, 2.5MW, H-mode; Green: #38159, D→ H, 2.5MW, L-mode; Blue: #36760, H → H, 2.8MW, L-mode; Black: #36270, D → D, 2.5MW, L-mode. The current is 800kA in all discharges, except #36270 (700kA) that for higher current transitions into H-mode as in #36267. Stable flat-top conditions with approximately constant core density and temperature (in particular for the D → H cases) could be established. Right top: ion and electron temperatures for selected time points (see fig. 2) in the flat-top phase. Right bottom: safety factor profiles (IDA) for the same time points.

In fig. 1 the time traces of three different L-mode and one H-mode discharges are shown. The magnetic field is $B_T = -2.5T$, the currents are limited to $700 - 800kA$ in order to avoid q=2 sawtooth-like crashes and transitions to H-mode, in particular for the D → D cases. After the current ramp-up phase, stationary conditions from $1.7s - 5s$ could be established. NB beam blips with a duration of 12 ms for diagnostic purposes (in particular T_i) can be seen in the central T_e channel and the plasma β_N traces. Since for H injection the maximum beam energy is limited to $72keV$ and $1.4MW$ per beam source, two off-axis sources (6 and 7, in total $2.8MW$) with similar injection angle were switched on in the flat-top phase in order to compare to the $2.5MW$ cases for D injection. Due to the different H-mode threshold in H, the H discharges stay in L-mode, even when $5MW$ of off-axis heating power is applied (#38160, not shown here).

Although the ramp-up phases were executed identically, different q-profiles in the flat-top phase develop (fig. 1). Also, the T_e and T_i profiles show a variety of different shapes: T_e is inverted in most cases due to the core impurity accumulation, whereas T_i is either inverted or monotonic.

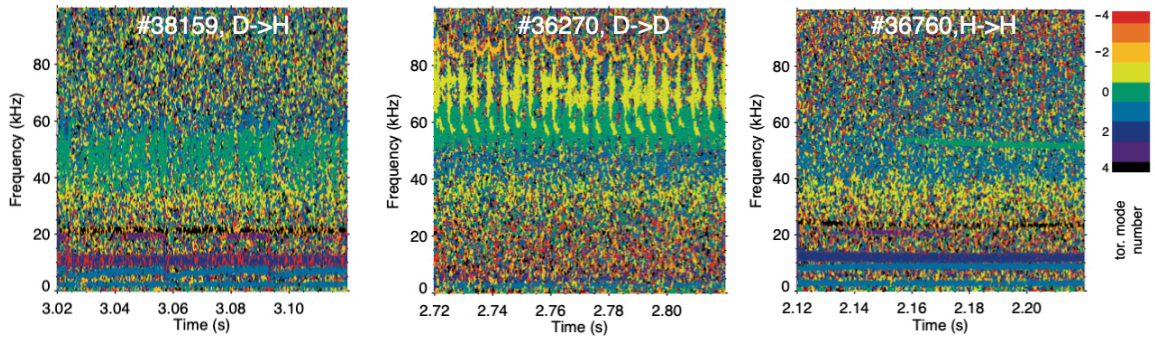

FIG. 2. Toroidal mode number analysis (NTI wavelet analysis tool [2]) of 3 discharges with similar heating power in a 100ms window during the flat-top phase. The different linear and non-linear features of EGAMs (green colour indicating n=0 modes) with an onset frequency of 50-60kHz and counter- propagating BAEs with similar frequency (n=-1 yellow, n=-2 orange) can be observed. In blue/violet: zero-frequency MHD modes located at $q = 2, 3$ rational surfaces.

As can be concluded from the toroidal mode analysis using magnetic pick-up coils (fig. 2, employing the NTI wavelet tool embedded in MTR [2]), EGAMs (green), RSAE, BAEs and TAEs [1] in ion (positive mode numbers, blue colors) and electron (negative mode numbers, yellow colors) diamagnetic directions can be observed. The typical frequency ranges are 50kHz for EGAMs, BAEs and RSAEs, and 100-150kHz for TAEs. As previously shown [1], the pitch-angle anisotropy of the NB distribution functions drives the EGAMs. Interestingly, a large variety of non-linear behaviour can be observed for different isotope mixes. In most of the previous discharges, especially during ramp-up, the EGAMs show a hook-like up-chirping (see also NLED base case [3] and ref. [1]). The EGAMs in the flat-top discharges with comparable heating powers show in addition also steady-state, (H→H, see fig. 2 right), dominant down-chirping (see fig. 2 middle), or symmetrical chirping behaviour (see fig. 2 left). Interestingly, the GAM continumm alone does not explain this observation: using an analytical expansion of the LIGKA-implemented gyro-kinetic dispersion relation [4, 5] with an elongation (κ) correction [6, 7] allows us to compare the onset frequency with the GAM continuum (see fig. 3). Experimental ion and electron temperature profiles as shown in fig. 1 at $2.5-3s$ are used to evaluate the GAM continuum frequency according to the following equation:

$$\omega_{GAM}^2 = q^2\omega_{t,i}^2\frac{2}{1+\kappa^2}\left[\left(\frac{7}{4}+\frac{T_e}{T_i}\right)+\left(23/8+2\tau+1/2\tau^2\right)/(\omega_{GAM}/\omega_{t,i})^2 - i\pi(\omega_{GAM}/\omega_{t,i})^5 exp\left\{-(\omega_{GAM}/\omega_{t,i})^2[1+(1+2T_e/T_i)/(\omega_{GAM}/\omega_{t,i})^2]\right\}\right] \quad (1)$$

with $\omega_{t,i} = v_{t,i}/(qR)$, $\tau = T_e/T_i$ and $v_{t,i} = \sqrt{2T_i/m_i}$ the thermal velocity of the ions.

In fig .3, the experimental frequencies at onset (lines) and the chirping ranges (arrows; no arrow if there is no chirping) are over-plotted. Their radial localisation as estimated from soft-X-ray (SXR) and reflectometry measurements correspond roughly to the extension of the lines. (For H-mode discharges with flat profiles, however, this localisation is not possible with reflectometry and relies only on SXR.) For discharges with low-f GAM continua, the continua act like a lower limit for the EGAM evolution (hook-like up-chirping), whereas for the H discharges and #36270 ($q < 2$ for $s < 0.6$), the EGAMs emerge 'within' the GAM continuum and chirp symmetrically or predominantly downwards. This confirms the 'energetic particle mode character' (EPM) [8] of EGAMs, i.e. their existence is almost exclusively determined by the steepest gradients of the EP distribution function (see fig.15 of ref. [9]). However, the damping at these locations in phase space - in particular due to the exponential q-dependence - cannot be too large. Note that the damping rate γ/ω due to the isotope effects alone does not change in formula 1, since the mass dependence cancels in $(\omega_{GAM}/\omega_{t,i})$. Thus, the details of the EP distribution function gradients in combination with the q-profile determine the strength of the effective EGAM drive and its non-linear behaviour (see also fig. 5).

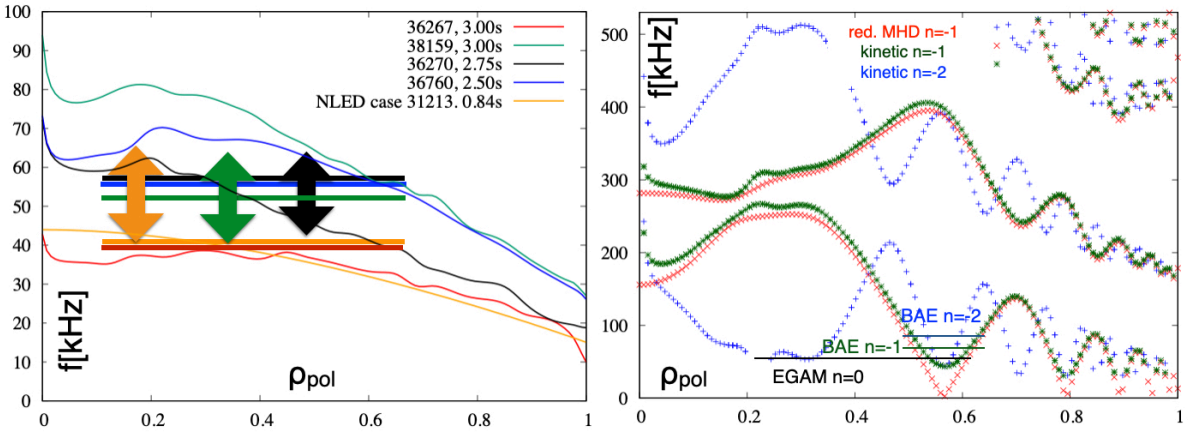

FIG. 3. Left: GAM continuum as calculated by formula 1 for the discharges and profiles shown in fig. 1 with the same color code. The onset EGAM frequencies and the experimentally estimated radial width are indicated by the corresponding bars. The arrows (same color code) indicate the chirping range. Right: reduced MHD continuum and kinetic continua for $n = 1, 2$ for discharge #36270 at 2.75s. The observed $n = 0, -1, -2$ perturbations as seen in fig. 2 middle and fig. 4 left, are indicated by the bars in the corresponding colors.

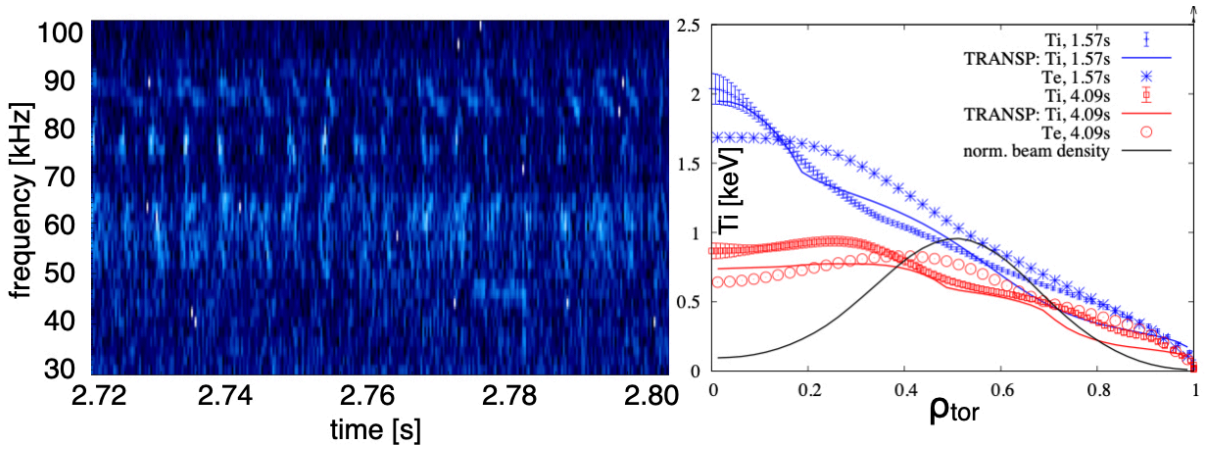

FIG. 4. Left: reflectometry measurements D→D discharge #36270 at $t = 2.75s$ (same time window as in fig. 2, middle). The cut-off layer of this channel (36GHz) corresponds to a localisation around $\varrho_{pol} \sim 0.5 - 0.6$. Right: D→D discharge #36267: comparison of the T_i profiles as measured at the onset of the beam blips at $t = 1.57s$ and $t = 4.09s$ and the TRANSP/NUBEAM predicted profiles. The normalised EP density profile is shown in black.

In pure H discharges no TAEs or BAEs can be observed. This is expected since the maximal injection energy is too low drive TAEs via the $v_A/3$ resonance, and for the q-profiles in fig. 1 no suitable BAE resonant surfaces for low n's are present in the steep EP gradient region. In fig. 3, right, the $n = 1$ and $n = 2$ kinetic continua for the D→D discharge #36270 at $t = 2.75s$ as calculated by the LIGKA code [10] are plotted. For comparison, the reduced MHD spectrum for $n = 1$ is shown as well. Using the information about the measured radial location (see fig. 4) and the frequency, one can conclude that the modes are kinetic BAEs that are localised close to the $q = 2$ rational surface. Global LIGKA calculations for this case (not shown here) confirm the existence of k-BAEs above the BAE/GAM accumulation point.

By comparing FIDA measurements with classical predictions it had been demonstrated that in these scenarios EPs are transported inwards [1]. By carrying out interpretative TRANSP/NUBEAM [11, 12] runs (using a gyro-Bohm model for ion heat transport) for the D→D discharge #36267 it has been found that the T_i profiles as given by TRANSP under-predict the measured values in the core significantly when strong mode activity is present (see fig. 4, $t = 4.09s$). At $t = 1.57s$ instead, in a quiescent phase, measured and simulated T_i profiles match closely in the core. Also, different T_e/T_i ratios in the two phases can be observed. Obviously, additional ion core heating mechanisms are not accounted for in the simulations. Note that the discrepancies mainly arise for $\varrho_{tor} < 0.4$ whereas for $0.4 < \varrho_{tor} < 0.7$ the profiles and gradients match. This finding leads to the hypothesis that the redistributed EPs affect the core temperature of the background ions. A similar study for the current/q-profiles is planned with optimised MSE/IMSE measurements.

Although several time points of this database were already modelled by various codes [1, 13, 9], the large variety of observed instabilities and transitions between different phases strongly motivates an automated analysis. To this end the LIGKA/HAGIS codepackage was recently implemented into the IMAS infrastructure and a python workflow (WF) for EP stability analysis was established [14]. For ITER scenario simulations this WF is already in an advanced stage (see below). For ASDEX Upgrade (AUG) the WF needs to be further adopted (profile fitting etc) before it can be applied to the experimental data base.

4. RAMP UP PHASE OF A JT-60SA SCENARIO WITH OFF-AXIS NB DEPOSITION

The exploration of scenarios with off-axis NB deposition leading to non-inductive steady-state operation at high β is one of the main missions of the JT-60SA project [16]. The high-energy negative ion sources ($\lesssim 500$ keV) at JT-60SA deposit exclusively off-axis. An exhaustive kinetic-hybrid MHD analysis using the MEGA code has been performed in refs. [17, 18, 19]. In order to compare and extend this analysis with GK linear simulations, an interface between the MEGA-generated EP distribution functions and LIGKA has been developed. The EP distribution as given by 7 million markers is binned, smoothed and splined to the LIGKA internal constants of motion space (see fig. 5). Special care is needed to exactly align the volume elements, in particular close to the magnetic axis. Small differences in the equilibrium need to be avoided for this reason.

For this study the MHD-relaxed q-profile at $t = 6s$ [18] was chosen and slightly up-shifted ($q_0 = 1.27$) to avoid multiple $q = 2$ surfaces. Three $n = 2, m = 4$ TAE surfaces remain ($q_{TAE} = 2.25$). An automated set of hierarchical analysis steps using the LIGKA code are carried out for even and odd TAEs with $n = 1 - 10$. First, the TAE

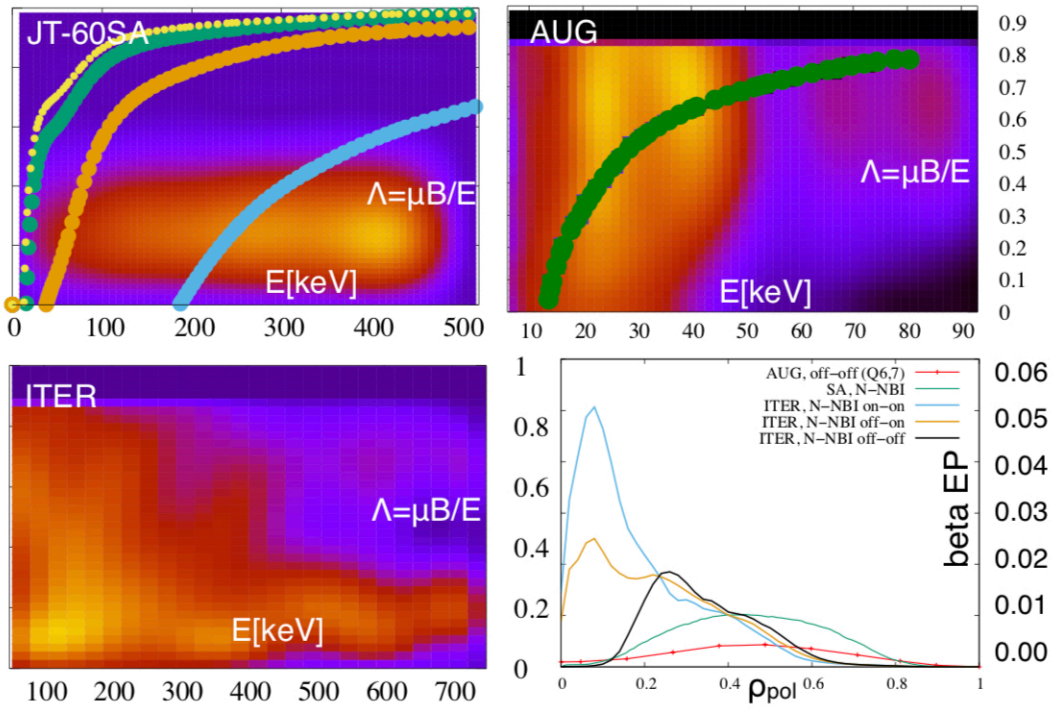

FIG. 5. Left top: normalised distribution function for the JT-60SA (see text) at $\varrho_{pol} = 0.4$ as function of E and $\Lambda = \mu B/E$. Various resonances are shown: for co-propagating modes the blue line indicates the main TAE resonance for $n = 2, m = 4, f = 85kHz$.Green: GAM/BAE resonance; for counter-propagating modes, no TAE resonances cross the densely populated phase space; $n = 2, m = 4, 5$ are shown in orange and beige for the counter propagating mode ; Right top: normalised distribution function for AUG 5MW flat-top case at $\varrho_{pol} = 0.4$ (#36267) with GAM/BAE resonance; Left bottom: ITER off/off-axis N-NB case based on METIS and ITER heating and current drive WF analysis [15] #100015 run 29 at $\varrho_{pol} = 0.4$; Right bottom: β_{EP} for three cases in the figure. Here also off/on and on/on-axis cases for the two ITER beam lines are added.

frequencies, radial location and radial mode width are estimated using analytical formulae (called LIGKA 'mode5' see fig. 7). This step is very fast and takes less than $2s$ for all modes under consideration (see fig. 6 for even and odd TAEs). Then the GK dispersion relation [20, 21] at the extrema of the TAE gaps (lower gap for even TAEs, upper gap for odd TAEs) is solved, providing ion and electron Landau damping rates (called LIGKA 'mode4'). Together with an analytical estimate for the radiative damping [22] this step provides in most cases a lower limit for the overall AE damping (continuum damping excluded, but also other non-local modifications and sidebands are neglected). This step takes about $10s$ per mode. Then, the global problem is solved (antenna method) [21]. Depending on the size of the radial and poloidal harmonics this step takes a few minutes using analytical estimates for the kinetic coefficients [4]) or up to $2h$ for HAGIS-precalculated kinetic data (called LIGKA 'mode1'). In fig. 6 (right) some examples for global even and odd TAEs, and an EAE are shown. As predicted by the local estimate, the multiple ($n = 2; m = 4, 5$) TAEs overlap radially, and form global eigenfunctions with weak damping (see blue mode in fig. 6 at $85kHz$ with $\gamma/\omega \sim 0.5\%$). The core-localised $n = 2; m = 3, 4$ TAE in the steep inverted gradient region is more heavily damped (lower q, larger T_i, larger shear). On the first glance, comparing β_{EP} to the AUG cases in section 3 (see fig. 5 right bottom) may suggests that the positive gradient in the core would destabilise these $n = 2$ TAEs, leading to counter propagating modes, as measured in the AUG cases above. However, a resonance analysis explains why no unstable TAE in the inner gap was found: for TAE frequencies (around $100 - 150kHz$) the resonance condition $\omega - \omega_D - (nq - m + k)\omega_t = 0$ cannot be fulfilled by co-passing particles of the populated beam region, at least not for the main TAE harmonics $m = 4, 5$. Here, ω_D is the precession drift and ω_t the transit frequency of the EPs. The resonance lines (i.e. the solution of the equation above) for the $n = 2; m = 4, 5$ TAE are plotted in orange and beige in fig. 5. The co-propagating $n = 2$ TAE instead has a principle resonance and thus can be destabilised by the negative EP gradient. Although not yet investigated in detail, this analysis suggests that due to their higher frequency counter propagating EAEs will be unstable and thus might be able to deplete the positive EP gradient. It should be noted, that with additional off-axis P-NB beams this conclusion might not hold since the lower energy region where TAE resonances can be found will be more densely populated.

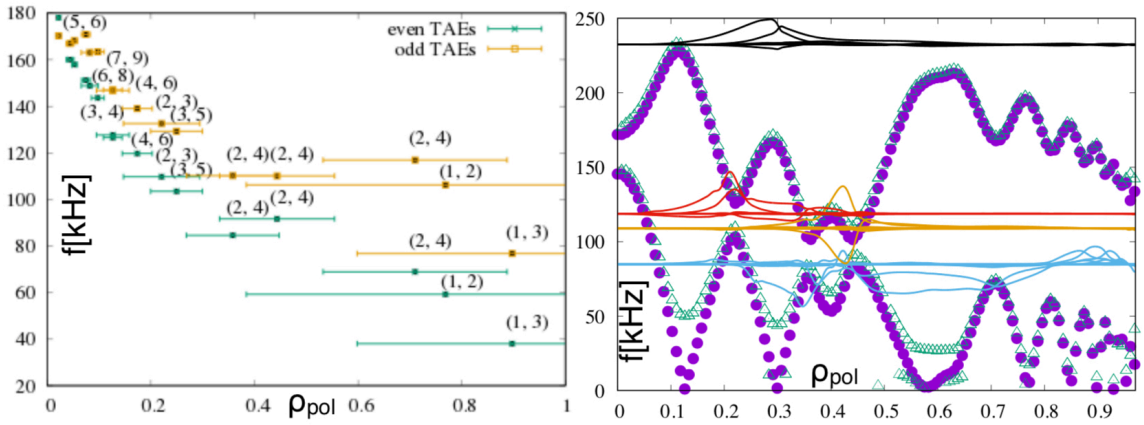

FIG. 6. Left: Frequency and estimated radial mode width for the JT-60SA case (see text) for n = 1...10 as calculated by a fast LIGKA analysis. Even (green) and odd (orange) TAEs are shown and labelled with the respective mode number (n, m); Right: reduced MHD (violet), kinetic spectrum (green) and selected weakly damped global modes (TAEs in various gaps in blue, red, orange, EAE in black) for n=2.

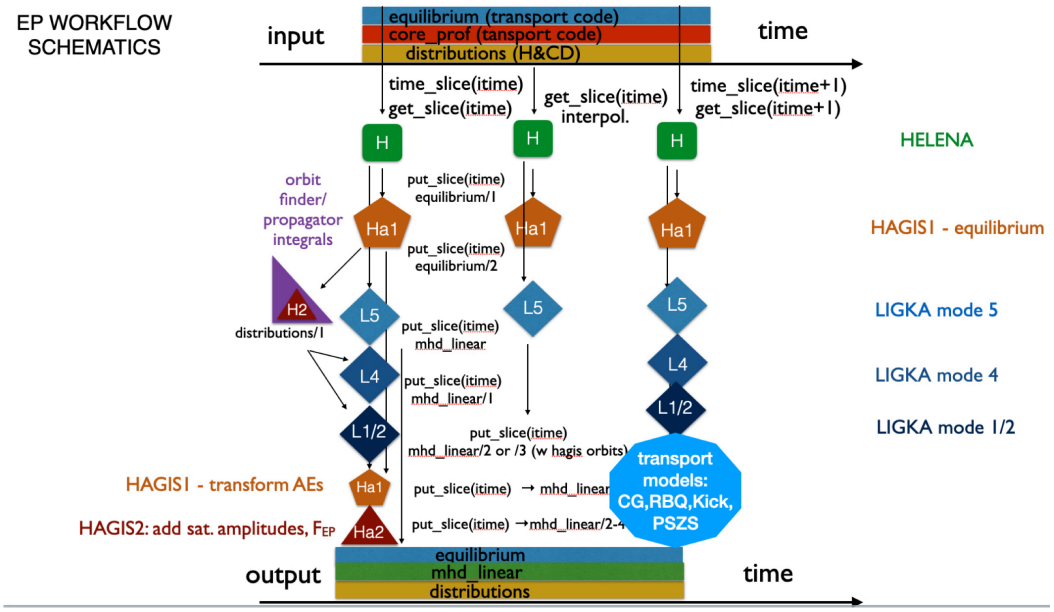

FIG. 7. Schematic layout of the EP stability WF: equilibrium, profile and EP distribution data is read from the IMAS data base and processed via HELENA [24] , the various LIGKA 'modes' up to HAGIS [25, 26]. In the future various EPs transport models can replace HAGIS for determining the quasi-linear or non-linear EP resditribution due to AEs.

Obviously, this analysis very much depends on the details of the q-profile in the core. For example, when q is assumed to be as flat as in the AUG cases, some TAEs gaps will fully align and then may allow for weakly damped modes with extended mode structures. In order to investigate this sensitivity, a time dependent analysis for a series of equilibria has to be carried out. In the next section we report on this new development, that presently is only available for ITER cases using the IMAS infrastructure [15, 23].

5. ITER PRE-FUSION PLASMA

During the lifetime of ITER various scenarios with off-axis NB injection are forseen. Although a change of the beam geometry from on-axis to off-axis will be possible, it cannot be performed frequently since the cycles are limited due to the mechanical stress it induces on the various components connected to the beam source. For this reason a good understanding of the expected heating characteristics and deposition properties including a possible deposition broadening due to EP-driven instabilities can help to optimise the planning and operation of

the experiments. Based on the fully IMAS [15] integrated heating and current drive (H&CD) WF [23] the stability of a pre-fusion H-plasma ($5MA/1.8T$, PFPO-2, #100015) is investigated for different beam deposition locations (off-axis, mixed on/off-axis). The beam β's for the three configurations (on/on, off/on, off/off) are shown in fig. 5, bottom right. Similarly to the MEGA interface described above, the particle-based EP distribution function as given by the H&CD WF (1 million markers) is processed and projected into the LIGKA constants of motion space. The result is shown in fig. 5, bottom left. As in the AUG and JT-60SA cases, phase space gradients and spatial gradients in both positive and negative directions arise. Due to the different injection angles, however, the deposition pattern varies considerably between the three experiments. Setting up this inter-machine comparison allows us to test our numerical tools for very different regions of the parameter space, as exemplified in fig. 5 and validate their range of applicability without loosing the direct contact to experimental data (AUG).
Next, the spectrum of potentially unstable modes has to be determined. To this end a time-dependent WF built on the ITER IMAS infrastructure has been created. It is written in Python and makes use of a simple interface that facilitates the parameter configuration for both the connection to the IMAS Database (for saving/retrieving data) and for the numerical codes themselves through a series of XML files. The general WF layout is shown in fig. 7. As described above, a series of hierarchical models implemented in LIGKA is applied to the time-dependent output of a transport code (or in the future directly to experimental data). Presently, BAEs, RSAEs, odd/even TAEs and odd/even EAEs are fully supported. The extension to other type of perturbations is in progress. In fig. 8 the results of a time-dependent run based on #100015, run 1 are shown. The frequencies of various AEs can be followed as a function of time. When plotting the radial locations, the importance of the q-profile evolution (and tailoring) becomes obvious: especially for flat q-profiles just above $q > 1$ no AE surfaces with reasonable low mode numbers ($n < 35$, compare also [27, 28, 29]) align with the steep negative gradient region between $\varrho_{pol} \sim 0.4 - 0.6$. The stability of these 'hybrid' scenarios with respect to EP stability will be further investigated in the future.

6. CONCLUSIONS AND OUTLOOK

In this paper we have summarised our recent efforts for establishing a set of tools targeted to the automated linear and non-linear analysis of EP stability and transport. For validation, a dedicated experimental effort on AUG has been reported that provides now an excellent data base for comprehensive modelling under stationary conditions in various isotope mixes. First steps to investigate their impact on transport and current drive are reported. This data-base extension was motivated and linked to two Eurofusion Enabling Research projects [31, 32], and in particular by a non-linear benchmark and validation exercise [13] based on the NLED case #31213 at $t = 0.84s$ [33], a predecessor of these flat-top studies, including the codes HYMAGYC, MEGA and ORB5 (see refs. in [13]).
As indicated in fig. 7, the application of this WF opens the possibility to connect to various reduced transport models (RTMs) [34, 35, 36, 37]. Since mode structures, frequencies and damping rates are a critical pre-requisite to all RTMs, the WF can be used in many different ways to provide these ingredients with different fidelity. At the same time, saturation amplitudes for single modes as provided by HAGIS, or the non-linear EP redistribution in a

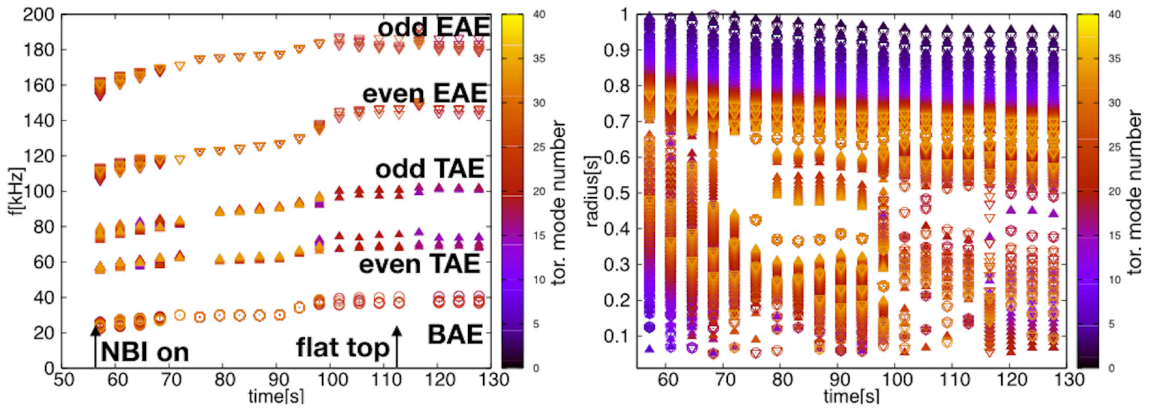

FIG. 8. Left: evolution of various (stable and unstable) Alfvén eigenmode (AE) frequencies as a function of time during the ramp-up of a H-plasma in ITER as calculated by the LIGKA/HAGIS WF based on a predictive METIS [30] run (#100015,1; $B_0 = -1.79T$). All modes in the negative EP gradient region between $0.35 < s < 0.55$ are shown. Right: the same dataset showing the evolution of the radial AE localisation with time. Regions of scarce AE population can be related to regions of low shear close to q=1.

multi-mode scenarios can be consistently calculated for verification and validation of the RTMs. Coupling to the RABBIT [38] code is planned to further speed up the WF. Also mode symmetry breaking effects and its impact on EP transport can be consistently included [39, 40]. Finally, the successful comparison of HAGIS/LIGKA in the appropriate limits to fully global gyro-kinetic simulations with ORB5 for ITER [29, 41] connects our workflow to the next higher level of the model hierarchy.

Acknowledgements: This work has been carried out within the framework of the EUROfusion Consortium and has received funding from the Euratom research and training programme 2014-2018 and 2019-2020 under grant agreement No 633053 and IO Contract No. IO/18/CT/4300001657. The views and opinions expressed herein do not necessarily reflect those of the European Commission. Part of this work has been supported by the following Enabling Research projects: CfP-AWP17-ENR-MPG-01 (Ph. Lauber), CfP-AWP19-ENR-ENEA-01 (F. Zonca), ENR-MFE19.MPG-01 (G. Conway). ITER is the Nuclear Facility INB no. 174. The views and opinions expressed herein do not necessarily reflect those of the ITER Organisation.

REFERENCES

[1] Ph Lauber et al 2018 *EX/1-1 Proc. 27th IAEA FEC, 22-27 October 2018, Gandhinagar (Ahmedabad) Gujarat, India.*
[2] Horváth L, Poloskei P Z, Papp G, Maraschek M, Schuhbeck K H, Pokol G I and and 2015 *Plasma Physics and Controlled Fusion* **57** 125005
[3] F Zonca et al 2015 Wiki pages of the Eurofusion Enabling Research Project CfP-AWP15-ENR-ENEA-03: Nonlinear Energetic Particle Dynamics (NLED) project URL `https://www2.euro-fusion.org/ERwiki/index.php?title=ER15-ENEA-03`
[4] Lauber P and Lu Z 2018 *Journal of Physics: Conference Series* **1125** 012015
[5] Bierwage A and Lauber P 2017 *Nuclear Fusion* **57** 116063
[6] Zonca, F and Chen, L 2008 *EPL* **83** 35001
[7] Gao Z, Peng L, Wang P, Dong J and Sanuki H 2009 *Nuclear Fusion* **49** 045014
[8] Chen L and Zonca F 2016 *Rev. Mod. Phys.* **88**(1) 015008
[9] Horvath L, Papp G, Lauber P, Por G, Gude A, Igochine V, Geiger B, Maraschek M, Guimarais L, Nikolaeva V, Pokol G and the ASDEX Upgrade Team 2016 *Nuclear Fusion* **56** 112003
[10] Lauber P, Günter S, Könies A and Pinches S D 2007 *Journal Of Computational Physics* **226** 447–465
[11] PPPL 2018 for TRANSP references see URL `https://w3.pppl.gov/tftr/transp/refs`
[12] Pankin A, McCune D, Andre R, Bateman G and Kritz A 2004 *Computer Physics Communications* **159** 157 – 184
[13] G Vlad et al 2021 *Proc. 28th IAEA FEC, 10-15 May 2021, Nice, France.*
[14] Popa V A 2020 *Master Thesis, TU München*
[15] SD Pinches et al 2018 *TH/P6-7 Proc. 27th IAEA FEC, 22-27 October 2018, Gandhinagar (Ahmedabad) Gujarat, India.*
[16] JT-60SA Research Unit 2018 JT-60SA Resarch Plan v4.0 URL `https://www.jt60sa.org/b/index.htm`
[17] Toma M, Hamamatsu K, Hayashi N, Honda M and Ide S 2015 *Plasma Physics and Controlled Fusion* **57** 095007
[18] Bierwage A, Toma M and Shinohara K 2017 *Plasma Physics and Controlled Fusion* **59** 125008
[19] Bierwage A, Aiba N, Matsuyama A, Shinohara K and Yagi M 2018 *Plasma Physics and Controlled Fusion* **61** 014025
[20] Zonca F, Chen L and Santoro R 1996 *Plasma Physics and Controlled Fusion* **38** 2011–2028
[21] Lauber P 2013 *Physics Reports* **533** 33 – 68
[22] Pinches S D, Chapman I T, Lauber P W, Oliver H J C, Sharapov S E, Shinohara K and Tani K 2015 *Physics of Plasmas (1994-present)* **22** 021807
[23] SD Pinches et al 2021 *Proc. 28th IAEA FEC, 10-15 May 2021, Nice, France.*
[24] Huysmans G, Goedbloed J and Kerner W 1991 *Proc. CP90 Conf. on Computational Physics* p p 371
[25] Pinches S D, Appel L C, Candy J, Sharapov S E, Berk H L, Borba D, Breizman B N, Hender T C, Hopcraft K I, Huysmans G T A and Kerner W 1998 *Computer Physics Communications* **111** 133–149
[26] Pinches S 1996 *Ph.D. Thesis, The University of Nottingham*
[27] Lauber P 2015 *Plasma Physics and Controlled Fusion* **57** 054011
[28] Schneller M, Lauber P and Briguglio S 2016 *Plasma Physics and Controlled Fusion* **58** 014019
[29] Hayward-Schneider T, Lauber P, Bottino A and Lu Z 2021 *Nuclear Fusion* **61** 036045
[30] Artaud J, Imbeaux F, Garcia J, Giruzzi G, Aniel T, Basiuk V, Bécoulet A, Bourdelle C, Buravand Y, Decker J, Dumont R, Eriksson L, Garbet X, Guirlet R, Hoang G, Huynh P, Joffrin E, Litaudon X, Maget P, Moreau D, Nouailletas R, Pégourié B, Peysson Y, Schneider M and Urban J 2018 *Nuclear Fusion* **58** 105001
[31] Ph Lauber et al 2017 Wiki pages of the Eurofusion Enabling Research Project CfP-AWP17-ENR-MPG-01: Nonlinear interaction of Alfvénic and turbulent fluctuations in burning plasmas (NAT) URL `https://www2.ipp.mpg.de/~pwl/NAT/ENR_NAT.html`
[32] F Zonca et al 2020 Wiki pages of the Eurofusion Enabling Research Project CfP-AWP19-ENR-01: Nonlinear Energetic Particle Dynamics (NLED) project URL `https://www.afs.enea.it/zonca/METproject/Activities.html`
[33] Ph Lauber 2015 The NLED base case URL `https://www2.ipp.mpg.de/~pwl/NLED_AUG/data.html`
[34] Podestà M, Gorelenkova M and White R B 2014 *Plasma Physics and Controlled Fusion* **56** 055003
[35] Carlevaro N, Falessi M V, Montani G and Zonca F 2015 *Journal of Plasma Physics* **81** 495810515
[36] Gorelenkov N, Duarte V, Podesta M and Berk H 2018 *Nuclear Fusion* **58** 082016
[37] Falessi M V and Zonca F 2019 *Physics of Plasmas* **26** 022305 (*Preprint* `https://doi.org/10.1063/1.5063874`)
[38] Weiland M, Bilato R, Dux R, Geiger B, Lebschy A, Felici F, Fischer R, Rittich D, van Zeeland M and and 2018 *Nuclear Fusion* **58** 082032
[39] Lu Z, Wang X, Lauber P and Zonca F 2018 *Nuclear Fusion* **58** 082021
[40] Meng G, Lauber P, Lu Z and Wang X 2020 *Nuclear Fusion* **60** 056017
[41] T Hayward-Schneider et al 2021 *Proc. 28th IAEA FEC, 10-15 May 2021, Nice, France.*